Production of Offspring from Azoospermic Mice with Meiotic Failure: Precise Biparental Meiosis within Halved Oocytes

Narumi Ogonuki[1], Hirohisa Kyogoku[2,3], Toshiaki Hino[4], Yuki Osawa[5], Yasuhiro Fujiwara[6], Kimiko Inoue[1,7], Tetsuo Kunieda[8], Seiya Mizuno[9], Hiroyuki Tateno[4], Fumihiro Sugiyama[9], Tomoya S. Kitajima[2]*, Atsuo Ogura[1,7,10]*

[1]Bioresource Engineering Division, RIKEN BioResource Research Center, Ibaraki 305-0074, Japan.

[2]Laboratory for Chromosome Segregation, RIKEN Center for Biosystems Dynamics Research, Kobe, Hyogo 650-0047, Japan.

[3]Graduate School of Agricultural Science, Kobe University, Kobe, Hyogo 657-8501, Japan.

[4]Department of Biological Sciences, Asahikawa Medical University, Asahikawa, Hokkaido 078-8510, Japan.

[5]Graduate School of Comprehensive Human Sciences, University of Tsukuba, Tsukuba, Ibaraki 305-8575, Japan.

[6]Laboratory of Pathology and Development, Institute for Quantitative Biosciences, The University of Tokyo, Yayoi, Bunkyo-ku, Tokyo 113-8657, Japan.

[7]Graduate School of Life and Environmental Sciences, University of Tsukuba, Tsukuba, Ibaraki 305-8572, Japan.

[8]Faculty of Veterinary Medicine, Okayama University of Science, Imabari, Ehime 794-8555, Japan.

[9]Laboratory Animal Resource Center and Trans-border Medical Research Center, Faculty of Medicine, University of Tsukuba, Tsukuba, Ibaraki 305-8575, Japan.

[10]RIKEN Cluster for Pioneering Research, Wako, Saitama 351-0198, Japan.

*Correspondence: tomoya.kitajima@riken.jp and ogura@rtc.riken.go.jp

While the large volume of mammalian oocytes is necessary for embryo development, it can lead to error-prone chromosomal segregation during meiosis. Conversely, we hypothesized that smaller oocytes would have a great unidentified potential to stabilize unstable meiosis and improve the development of the resultant embryos. Here, we show that reducing ooplasmic volume can rescue highly error-prone fertilization using primary spermatocytes by preventing segregation errors of chromosomes during biparental meiosis. High-resolution live-imaging analysis revealed that erroneous chromosome segregation occurred in most (90%) spermatocyte-injected oocytes of normal size, but could be ameliorated to 40% in halved oocytes. The birth rate improved remarkably from 1% to 19% (*P* < 0.0001). Importantly, this technique enabled the production of offspring from azoospermic mice with spermatocyte arrest caused by STX2 deficiency, an azoospermia factor also found in humans. Thus, contrary to popular opinion, oocytes inherently have a strong potential for precise meiotic divisions, which can be evoked by reduction of the ooplasmic volume. Their potential might help rescue cases of untreatable human azoospermia with spermatocyte arrest. (170 words)

Keywords: azoospermia; fertilization; meiosis; oocyte; spermatocyte

52 **INTRODUCTION**

53 Fertilization is the process whereby female and male gametes (oocytes and
54 spermatozoa) unite to form a zygote. From the standpoint of their genomes, the
55 oocyte and spermatozoon are equivalent, but their history and cell type are quite
56 different. Oocytes acquire their large cytoplasm (the ooplasm) during oogenesis
57 to store all the components necessary for embryogenesis, including organelles,
58 proteins, metabolites, mRNAs, and other molecules. By contrast, the
59 contribution of spermatozoa to zygote formation and embryonic development is
60 largely limited to deposition of the paternal genome and oocyte activation.
61 Consequently, simple injection of a spermatozoon or even the sperm head
62 (nucleus) into a mature oocyte results in normal fertilization, leading to embryo
63 development and birth of offspring (Ogura et al., 2005; Palermo et al., 1992).
64 Fertilization of oocytes does not even require mature sperm nuclei, because
65 injection of nuclei from immature spermatozoa (spermatids) is sufficient for
66 normal fertilization and embryo development to term (Ogura et al., 2005).
67 Indeed, in one clinical study, 90 babies were born following round spermatid
68 injection, without any significant adverse effects (Tanaka et al., 2018).
69 Therefore, a large ooplasm helps determine the embryo's
70 developmental potential. However, it is known that this feature does not always
71 provide benefits for development. We and others have shown that a large
72 ooplasm is linked to error-prone chromosomal segregation, by analyzing
73 high-resolution images of meiotic chromosomes in oocytes with artificially
74 increased or decreased ooplasmic volume (Kyogoku and Kitajima, 2017; Lane

75 and Jones, 2017). Thus, the evolution of a particular ooplasmic mass in a
76 species might have arisen as a delicate trade-off between meiotic fidelity and
77 post-fertilization developmental competence. In our analysis, it was clear that a
78 large ooplasm was detrimental, because the meiotic chromosomes showed
79 frequent abnormal behavior, which could have led to aneuploidy and embryonic
80 death. Conversely, one can postulate that a smaller ooplasm might be more
81 beneficial than a larger one in terms of chromosomal behavior, but there is no
82 evidence for this because intact oocytes undergo meiotic divisions normally
83 during oogenesis and fertilization in experimentally tractable animal models such
84 as mice.

85 As mentioned above, normal diploid embryos can be obtained using
86 spermatids because they are already haploid, as are mature spermatozoa.
87 However, the use of primary spermatocytes for fertilization is considered to be
88 ineffective because they are premeiotic germ cells. Theoretically, the
89 chromosomes of primary spermatocytes might be able to contribute to the
90 construction of diploid embryos after two meiotic divisions within oocytes.
91 Indeed, we and another group have reported the birth of mice following
92 spermatocyte injection into oocytes, but the success rates were low at 1% to 3%
93 per embryo transferred (Kimura et al., 1998; Ogura et al., 1998). This was mostly
94 caused by the death of embryos shortly after implantation. When we observed
95 the reconstructed oocytes at metaphase II (MII), there was a high incidence of
96 chromosomal aberrations (Miki et al., 2006; Ogura et al., 1998). Since then,
97 there have been no technical improvements in spermatocyte injection. However,
98 the use of primary spermatocytes for conception should be explored, given that

99 many cases of nonobstructive azoospermia in humans are associated with
100 spermatogenic arrest at the primary spermatocyte stage (Enguita-Marruedo et
101 al., 2019).

102 Based on these findings, we expected that reducing the ooplasmic volume
103 might improve the chromosomal integrity of spermatocyte-injected oocytes and
104 increase the survival rate of the resultant embryos. In this study, by employing
105 high-resolution live-imaging techniques, we analyzed the segregation patterns of
106 the maternal and paternal chromosomes within spermatocyte-injected oocytes
107 with or without reduction of the ooplasm. Furthermore, we examined whether
108 such reduction could improve the birth rate following spermatocyte injection and
109 whether this technology could be applied to azoospermic mice having a mutation
110 causing spermatocyte arrest.

111 RESULTS

112 Reduction of the Recipient Ooplasmic Volume Increases the Rate of 113 Normal Diploidy in Spermatocyte-injected Oocytes

114 Fertilization with primary spermatocytes was achieved by injecting a
115 spermatocyte nucleus into immature oocytes at the germinal vesicle (GV) stage
116 followed by arrest at the metaphase of meiosis I (MI) induced by cytochalasin D
117 treatment (**Figure 1A**). Here, the maternal and paternal (spermatocyte-derived)
118 chromosomes were synchronized, forming a single chromosomal mass. After
119 removal of cytochalasin D, they underwent meiotic division with protrusion of the
120 first polar body to reach the MII stage (**Figure 1A**). This reconstructed MII
121 “zygote” could be activated artificially to resume meiosis and form a one-cell

122 embryo having one zygotic nucleus (**Figure 1A**). To test the developmental
123 ability of reconstructed embryos, we transferred these MII chromosomes to
124 freshly prepared enucleated MII oocytes (Ogura et al., 1998).

125 Recipient oocytes with half the normal ooplasmic volume were prepared by
126 aspiration using a large glass pipette (**Movie S1**). Using these halved oocytes,
127 we first analyzed the chromosomal integrity of spermatocyte-injected oocytes. In
128 control oocytes without spermatocyte injection (i.e., oocyte chromosomes only),
129 the proportion of oocytes with normal chromosomes was 97% at MII (**Figure 1B**
130 **and Table S1**). In spermatocyte-injected oocytes with intact ooplasm, the
131 proportion of normal chromosomes was decreased significantly to 2% (1/59, $P <$
132 0.0001) (**Figure 1B and Table S1**). The most frequent abnormality (86%, 51/58)
133 was the presence of prematurely separated sister chromatids (**Figure 1B and**
134 **Table S1**). When spermatocytes were injected into half-sized oocytes, the
135 proportion of MII oocytes with normal chromosomes improved significantly to
136 13/62 (21%; $P < 0.005$, vs the intact cytoplasm group) because of the decreased
137 number of separated chromatids (**Figure 1B and Table S1**). Thus, while
138 chromosomal normality was largely lost during meiosis I in
139 spermatocyte-injected oocytes, chromosomal aberrations could be prevented in
140 a significant proportion of oocytes by reduction of the ooplasmic mass.

141 **Reduction of the Recipient Ooplasm Corrects the Behavior of**
142 **Spermatocyte-derived Chromosomes During Meiosis**

143 Next, we sought to study how chromosomal behavior was influenced by the
144 ooplasmic volume and which of the two parental (maternal or paternal)
145 chromosomes was more vulnerable to the stress of biparental meiosis. The

146 high-resolution three-dimensional (3D) live imaging system reported in our
147 previous studies was employed for analyzing the chromosomal behavior during
148 meiosis I (Kitajima et al., 2011; Kyogoku and Kitajima, 2017). To this end, it was
149 essential to discriminate the origins of the chromosomes via fluorescence
150 microscopy. Interestingly, the paternal (spermatocyte-derived) chromosomes
151 could be distinguished from the maternal chromosomes by the relatively lower
152 fluorescent intensities of the histone H2B-mCherry marker (**Figure 2A**). Our 3D
153 visualization of individual chromosomal positions showed that biparental meiosis
154 exhibited more frequent misalignment of paternal chromosomes at late MI,
155 compared with the maternal chromosomes (**Figures 2B, C and Movie S2**).
156 Halving ooplasmic volume significantly reduced the number of misaligned
157 paternal chromosomes (**Figures 2B, C and Movie S3**), an effect that we
158 expected based on our previous observations (Kyogoku and Kitajima, 2017).
159 Thus, paternal chromosomes are susceptible to errors in ooplasm-hosted
160 biparental meiosis, which can be tuned by reducing the ooplasmic volume.
161 We then analyzed how biparental meiosis in normal-sized ooplasms results
162 in chromosomal abnormality. Our technique of complete centromere tracking
163 using 3D imaging (Kitajima et al., 2011; Sakakibara et al., 2015) enabled us to
164 demonstrate that 89% of biparental meiotic divisions showed errors in
165 chromosomal segregation at anaphase I (**Figures 2B, 3A and Movie S2**).
166 Almost all of the errors were of spermatocyte origin (**Figure 3A**). Categorization
167 of anaphase trajectories showed that predominant error patterns were balanced
168 and unbalanced predivisions (premature segregation of sister chromatids at MI)

169 (**Figure 3B**), consistent with our observation of separated chromatids in MII
170 spreads (**Figures 1B and Table S1**).
171 Predivisions are error patterns observed following premature separation of
172 bivalent chromosomes into univalents during the prometaphase and metaphase
173 in naturally aged oocytes (Sakakibara et al., 2015). Therefore, we carefully
174 analyzed the prometaphase–metaphase trajectories of the chromosomes that
175 underwent segregation errors in biparental meiosis. This analysis revealed that
176 most of the errors were preceded by premature separation of bivalent
177 chromosomes into univalent-like structures (**Figures 2B, 3C and Movies S2,**
178 **S3**). Importantly, decreasing (halving) the recipient ooplasm mass significantly
179 suppressed the premature bivalent separation of chromosomes (75% in controls
180 vs 31% in halved oocytes) (**Figure 3D**) and chromosome segregation errors
181 (89% in control vs 46% in halved oocytes) (**Figures 3A, B, and D**). Thus, the
182 chromosomal aberrations found in spermatocyte-injected oocytes were largely
183 attributable to the premature separation of spermatocyte-derived chromosomes,
184 and about half of such aberrations could be prevented by reducing the size of
185 the recipient ooplasm (**Figure 3E**).

186 **Reduction in the Recipient Ooplasm Improved the Birth Rates Following**
187 **Spermatocyte Injection**

188 Next, we examined whether reduction of the ooplasm volume could improve the
189 developmental ability of spermatocyte-derived embryos. When we reconstructed
190 embryos using normal-sized oocytes and transferred them into recipient
191 females, only 1% (1/96) developed into offspring (**Figure 4A and Table S2**),
192 consistent with our previous reports (Miki et al., 2006; Ogura et al., 1998). By

193 contrast, when we used halved oocytes, 19% (17/90) of the reconstructed
194 embryos developed into live offspring, achieving a nearly 20-fold improvement
195 ($P < 0.0001$, **Figure 4A and Table S2**). The pups born by this improved method
196 had body and placental weights within the normal ranges (**Figure S1**). We
197 allowed three male pups to grow into adults and confirmed that they were all
198 fertile by mating them with normal female mice.

199 **Spermatocyte Injection Rescued Azoospermia Caused by Meiotic Arrest**

200 Finally, we applied this improved spermatocyte injection method to mouse
201 strains with azoospermia caused by spermatogenic arrest at the primary
202 spermatocyte stage. If the chromosomes of spermatocytes are functionally and
203 structurally intact, we surmised that their normal meiotic divisions might be
204 induced by the meiotic machinery of recipient oocytes. We performed our
205 studies on *Stx2*^{repro34} mice (hereafter, *repro34* mice) that carry a mutation in the
206 *Stx2* (syntaxin 2) gene induced by *N*-ethyl-*N*-nitrosourea (ENU) mutagenesis
207 (Fujiwara et al., 2013). Its human homologue, *STX2*, has been identified as a
208 causal factor of nonobstructive azoospermia (Nakamura et al., 2018). Both
209 mouse *Stx2* and human *STX2* mutations are characterized by the formation of
210 large syncytial spermatocytes because of their inability to maintain intercellular
211 bridges (Fujiwara et al., 2013; Nakamura et al., 2018) (**Figure 4B**). We
212 confirmed that the nuclei within these syncytial cells of *repro34* mice were
213 derived from spermatocytes by examining their prophase I chromosomes
214 following injection into MII oocytes (**Figure 4C**). We reconstructed embryos
215 using the nuclei collected from these syncytial spermatocytes (**Figure 4D and**
216 **Movie S4**). After 41 embryos were transferred into recipient females, five pups

217 (four female and one male) were born (**Figure 4E**). All of these pups carried the
218 point mutation in the *Stx2* gene (**Figure 4F**). We also applied this technique to
219 spermatocytes from *Exoc1* (exocyst complex component 1)-deficient mice that
220 also show syncytial spermatocytes (Osawa et al., 2021). Three pups (two female
221 and one male) carrying the mutation were born at term (**Figure S2**). All the eight
222 pups derived from *Stx2*- or *Exoc1*-deficient spermatocytes looked normal in
223 appearance and their body and placental weights were within normal ranges,
224 except for the body weight of pups from *Stx2*-deficient spermatocytes (**Figure**
225 **S1**). They grew into normal-looking adults and were proven to be fertile.

226 **Chromosomal Analysis of Offspring Born Following Spermatocyte**
227 **Injection**

228 As described above, all the pups born following the injection of wild-type
229 spermatocytes or mutant spermatocytes grew into fertile adults. We then
230 analyzed their chromosomal constitution in detail by multicolor fluorescence *in*
231 *situ* hybridization (FISH). Among the three male mice derived from wild-type
232 spermatocytes, two had a normal karyotype, but one had XYY sex
233 chromosomes (**Figure S3**). Among the five mice (four female and one male)
234 derived from *Stx2*-deficient spermatocytes, two female mice and one male
235 mouse were normal, but one female had an XO chromosome and another had a
236 shortened X chromosome (**Figure S4**). Among the three female mice derived
237 from *Exoc1*-deficient spermatocytes, one had an XO chromosomal
238 configuration. No abnormalities were found in the autosomes of the mice
239 examined.

240 **DISCUSSION**

241 Here, we addressed whether reducing the recipient ooplasm could ameliorate
242 the embryonic death rate caused by the meiotic errors that can occur in
243 mammalian oocytes. To this end, we employed an assisted fertilization system
244 using primary spermatocytes, which need simultaneous biparental meiosis
245 within oocytes: namely, meiosis with doubled chromosomes. Following
246 spermatocyte injection into halved oocytes, the proportion of normal
247 chromosomes at MII increased from 2% to 21% and the birth rate increased from
248 1% to 19%. These results demonstrate unequivocally that reducing the mass of
249 the ooplasm indeed helps to normalize chromosomal behavior, leading to better
250 survival of embryos to term. It would be interesting to test whether this strategy
251 could also correct the meiotic errors that are frequently found in oocytes from
252 aged female mammals (Mihajlović and FitzHarris, 2018). In humans, these
253 meiotic errors in oocytes are known to increase with advanced age and to
254 reduce conception rates significantly (El Yakoubi and Wassmann 2017; Mikwar
255 et al., 2020). In these errors, diverse mechanistic defects are involved, such as
256 defects in chromosomal cross-over formation, cohesin loss and spindle
257 deformation (Ma et al., 2020; Mihajlović and FitzHarris, 2018). We suspect that
258 reducing the mass of the ooplasm might help rescue or prevent at least some of
259 these defects.

260 The nearly 20-fold improvement in the birth rate following spermatocyte
261 injection into halved oocytes was much better than we expected. It is known that
262 meiosis in female and male mammals differs largely with respect to the

263 underlying molecular mechanisms and cell cycle progression patterns, such as
264 absence of the interphase between two meiotic divisions in female germ cells.
265 Consistent with this, many strains of gene knockout mice carrying mutations of
266 meiosis-related factors show male or female infertility (Biswas et al., 2021;
267 Jamsai and O'Bryan, 2011). Our findings imply that the meiotic chromosomes of
268 female and male germ cells have structural commonalities that allow
269 mechanistic interchangeability between them. Nevertheless, most chromosomal
270 aberrations were identified as of spermatocyte origin with a high incidence of
271 premature sister chromatid segregation during meiosis I. Most of these errors
272 were preceded by premature separation of bivalent chromosomes into
273 univalent-like structures. Our results reveal a novel effect of ooplasmic reduction
274 that can suppress premature separation of chromosomes, at least in the context
275 of biparental meiosis. These suggest that spermatocyte-derived chromosomes
276 are more vulnerable to physical or biochemical properties associated with a
277 large ooplasm, such as spindle size, and ooplasmic dilution of nuclear factors
278 (Kyogoku and Kitajima, 2017). The delayed alignment of spermatocyte-derived
279 chromosomes to the MI spindle (**Figures 2B and C**) might also reflect these
280 differences. In other words, maternal meiotic chromosomes might have evolved
281 special mechanisms that efficiently avoid segregation errors in a large ooplasm.
282 Chromosomal analysis by multicolor FISH revealed that four of the 11
283 spermatocyte-derived offspring carried chromosomal abnormalities that were
284 restricted to the sex chromosomes. There were no abnormalities in autosomes
285 in any of the mice analyzed. This sex-chromosome-biased chromosomal
286 aberration may be explained by the high embryonic lethality of autosomal

287 aneuploidy, which might have selected embryos with normal autosomes for
288 survival to term. It might also have resulted from yet undiscovered special
289 characteristics of sex chromosomes, especially those derived from
290 spermatocytes. All the abnormal patterns found in the sex chromosomes—XO,
291 XX with a shortened X, and XYY—can be explained by segregation errors of
292 spermatocyte XY chromosomes during meiosis I (see **Figures 3B and E**). It is
293 known that sex chromosomes are prepared to undergo meiosis later than
294 autosomes as they require the formation of the XY body (Kauppi et al., 2011).
295 Therefore, it is possible that spermatocytes that had not completed this stage
296 might have been selected for injection accidentally.
297 This study has practical implications for treating spermatogenic arrest
298 caused by meiotic arrest. Given the complexity of meiosis, many genes are
299 involved in its regulation, as revealed by mouse gene knockout models (Jamsai
300 and O'Bryan, 2011). Defects in some of these genes might cause failure of
301 meiosis and spermatogenic arrest at the primary spermatocyte stage. The
302 results of this study will help identify the types of meiotic arrest that can be
303 rescued or prevented by the spermatocyte injection technique we developed
304 here. Such information would provide invaluable clues for human clinical
305 research aiming to develop treatments for meiosis-related male infertility. In
306 addition, we propose another important implication of this study: at present,
307 complete *in vitro* gametogenesis is possible for female germ cells (Hikabe et al.,
308 2016), but not for male germ cells. One of the major causes of this sex-specific
309 difference in *in vitro* gametogenesis is the inability of male germ cells to undergo
310 meiosis *in vitro*. If male primordial germ cell-like cells derived from induced

311 pluripotent stem cells (Hayashi et al., 2011) could be cultured to form pachytene
312 spermatocytes, injecting them into immature oocytes as substitute gametes
313 might produce offspring by skipping *in vivo* male gametogenesis completely.
314 This could be the ultimate strategy to enable conception in cases of male
315 patients with germ cell loss. These scenarios could open up new methods for
316 treating human male infertility, although there are a number of ethical and
317 technical issues—for example, the high incidence of sex chromosome
318 abnormalities—that need to be resolved before these strategies could be used
319 by clinics offering assisted reproductive technology.
320

321 MATERIALS AND METHODS

322

323 Mice

324 All animal experiments were approved by and performed according to the
325 principles of the Institutional Animal Care and Use Committees at RIKEN,
326 Tsukuba and Kobe Branches. B6D2F1 and C57BL/6NCrSlc mice were
327 purchased from Japan SLC. ICR mice were purchased from CLEA, Japan.
328 *Repro 34* mice carrying the $Stx^{repro34}$ mutation were introduced from Okayama
329 University. The *repro34* mutation was induced in a C57BL/6J male and
330 subsequently a congenic line with the C3HeB/FeJ background was created
331 (Akiyama et al., 2008). Germline-specific *Exoc1* conditional knockout mice were
332 generated by breeding $Exoc1^{tm1c(EUCOMM)Hmgu}$ mice (Skarnes et al., 2011) with
333 *Nanos3*-Cre driver mice (kindly gifted by Dr Y. Saga, RIKEN BRC RBRC02568),
334 which express Cre in spermatogonia (Osawa et al., 2021; Suzuki et al., 2008).

335

336 **Collection of oocytes**

337 Female B6D2F1 mice (9–12 weeks old) were injected with 7.5 IU of equine
338 chorionic gonadotropin (eCG, ASKA Pharmaceutical, Tokyo,Japan). Forty-four
339 to forty-eight hours after injection, fully grown oocytes at the GV stage were
340 collected from large antral follicles and released into M2 medium supplemented
341 with 150 μg/ml dibutyryl cyclic (dbc) AMP (Merck KGaA). After being freed from
342 cumulus cells by pipetting, oocytes were cultured for at least 1 hours in MEM)
343 Merck KGaA) supplemented with 50 μg/mL gentamicin, 0.22 mM Na-pyruvate, 1
344 μg/ml epidermal growth factor (EGF), 150 μg/ml dbc AMP, and 4 mg/ml bovine
345 serum albumin (BSA), (mMEM) (Fulka and Langerova, 2014) at 37°C in an
346 atmosphere of 5% CO_2 in humidified air, until micromanipulation.

347

348 **Collection of primary spermatocytes**

349 Spermatogenic cells were collected from the testes of male B6D2F1, C57BL/6N,
350 and ICR mice (12–16 weeks old) by a mechanical method as reported in a
351 previous study (Ogura and Yanagimachi, 1993). Briefly, the testes were placed
352 in erythrocyte-lysing buffer (155 mM NH_4Cl, 10 mM $KHCO_3$, 2 mM EDTA; pH
353 7.2). After the tunica albuginea had been removed, the testes were transferred
354 into a cold (4°C) Dulbecco's phosphate-buffered saline (PBS) supplemented
355 with 5.6 mM glucose, 5.4 mM sodium lactate, and 3 mg/ml BSA (GL-PBS)
356 (Ogura et al., 1996). The seminiferous tubules were cut into small pieces using a
357 pair of fine scissors and pipetted gently to allow spermatogenic cells to be
358 released into the medium. The cell suspension was filtered through a 38-μm

359 nylon mesh and washed twice by centrifugation (200*g* for 4 min). After gentle
360 washing, the cells were resuspended in GL-PBS and stored at 4°C until
361 microinjection.
362
363 **Micromanipulation**
364 To make half-sized oocytes, oocytes at the GV stage were transferred to M2
365 medium (Merck Millipore) containing 7.5 μg/ml cytochalasin D (Merck KGaA)
366 and 60 mM NaCl for 10 min at 37°C. All manipulations were performed under an
367 inverted microscope with a Piezo-driven micromanipulator (PrimeTech). The
368 zona pellucida was opened by piezo drilling and one-third to half of the
369 ooplasmic volume was aspirated with an injection pipette (inner diameter 25 μm)
370 at 37°C (**Movie S1**). After manipulation, oocytes were cultured in mMEM
371 containing 7.5 μg/ml cytochalasin D and 40 mM NaCl at 37°C in an atmosphere
372 of 5% CO_2 in air. About 1–1.5 hours later, primary spermatocytes (pachytene to
373 diplotene stages) were injected into oocytes that were induced to arrest at the MI
374 stage by cytochalasin D. Oocytes were cultured in mMEM containing 7.5 μg/ml
375 cytochalasin D and 40 mM NaCl for 2 hours at 37°C in an atmosphere of 5%
376 CO_2 in humidified air. After washing in mMEM, the oocytes were cultured for 14–
377 17 hours until they reached the MII stage. The karyoplasts containing
378 chromosomes were removed and were then fused with fresh enucleated oocytes
379 using Sendai virus (HVJ; Ishihara Sangyo Co., Ltd.) in Hepes-buffered CZB
380 medium (Chatot et al., 1990) containing 7.5 μg/mL cytochalasin B. After
381 manipulation, the oocytes were cultured in CZB medium containing 7.5 μg/mL
382 cytochalasin B for 1 hours at 37°C in an atmosphere of 5% CO_2 in humidified air

383 until complete fusion occurred. Reconstructed oocytes were activated by
384 culturing them in Ca^{2+}-free CZB medium containing 8 mM $SrCl_2$ for 20 min. After
385 washing, the oocytes were cultured in CZB medium for 24 hours under 5% CO_2
386 in humidified air at 37°C.
387
388 **Embryo Transfer**
389 Embryos that reached the 2-cell stage by 24 hours were transferred into the
390 oviducts of Day 1 pseudopregnant ICR strain female mice (9–12 weeks old). On
391 day 19.5, recipient females were euthanized and their uteri were examined for
392 live fetuses. In some experiments, live fetuses were nursed by lactating foster
393 ICR strain mothers. After weaning, they were checked for fertility by mating with
394 ICR mice of the opposite sex.
395
396 **Chromosome preparation of oocytes**
397 The MII oocytes were treated with 0.5% actinase E (Kaken Pharmaceutical Co.)
398 for 5 min at room temperature to loosen the zona pellucida and then treated with
399 a hypotonic solution (1:1 mixture of 1.2% sodium citrate and 60% fetal bovine
400 serum, FBS; Merck KGaA) for 10 min at room temperature. Chromosome slides
401 were prepared using a gradual-fixation/air-drying method (Mikamo and
402 Kamiguchi, 1983). Briefly, oocytes were treated with Fixative I (methanol:acetic
403 acid:distilled water = 5:1:4) for 6–8 min and put onto a glass slide with a small
404 amount of Fixative I. Then, the oocytes were treated with Fixative II
405 (methanol:acetic acid = 3:1) for 2 min, followed by treatment with Fixative III
406 (methanol:acetic acid:distilled water = 3:3:1) for 1 min. The slides were air-dried

407 under conditions of 50%–60% humidity at 22–24°C. For conventional
408 chromosome analysis, the slides were stained with 2% Giemsa (Merck KGaA)
409 for 8 min. C-band staining was used to distinguish between structural
410 chromosome aberrations and aneuploidy (Tateno and Kamiguchi, 2007).
411
412 **Chromosome analysis by multicolor fluorescence *in situ* hybridization**
413 **(FISH)**
414 Spleens were removed under sterile conditions from mice produced by
415 spermatocyte injection. Lymphocytes were isolated from the spleen and
416 incubated in a tissue culture tube at a cell concentration of 1×10^6/ml in
417 RPMI1640 (Nacalai Tesque) containing lipopolysaccharide (10 μg/ml, Merck
418 KGaA), concanavalin A (3 μg/ml, Nacalai Tesque), 2-mercaptoethanol (50 μM,
419 Nacalai Tesque), and FBS (6%) at 37°C under 5% CO_2 in humidified air for 48
420 hours. Colcemid (KaryoMAX, Gibco) at a concentration of 0.02 μg/ml was added
421 to the cell suspension for the last 2 hours of culture to arrest the cell cycle at
422 metaphase. The cells were centrifuged at 420*g* for 5 min and resuspended in 3
423 ml of a hypotonic solution (0.075 M KCl). Twenty minutes later, 2 ml of Carnoy's
424 fixative (methanol:acetic acid = 3:1) was added to the cell suspension. Cells
425 were centrifuged at 420*g* for 5 min and resuspended in 5 ml of fresh Carnoy's
426 fixative. Centrifugations and fixations were repeated three times. Chromosome
427 preparations were made using a Hanabi metaphase spreader (ADSTEC). For
428 multicolor FISH analysis, the chromosome slides were hybridized with
429 21XMouse (MetaSystems) according to the manufacturer's protocol. For
430 denaturation of chromosomal DNA, the slides were incubated in 2 × saline

431 sodium buffer (SSC) at 70°C for 30 min and then treated with 0.07 M NaOH at
432 room temperature for 1 min. The denatured slides were washed in 0.1 × SSC
433 and 2 × SSC at 4 °C for 1 min each and dehydrated with a series of 70%, 95%,
434 and 100% ethanol. Multicolor FISH probes were denatured at 75°C for 5 min and
435 applied to the chromosome slides. After hybridization at 37°C for 48 hours in a
436 humidified chamber, the chromosome slides were treated with 0.4 × SSC at
437 72°C for 2 min, washed in 2 × SSC with 0.05% Tween20 (Merck KGaA) at room
438 temperature for 30 seconds, and rinsed in distilled water. For counterstaining,
439 the slides were covered by a coverslip with DAPI/Antifade (MetaSystems). The
440 chromosome slides were observed using fluorescent microscopy. Fluorescence
441 images were captured using a high-sensitive digital camera (α7s, SONY). The
442 images were imported into the ChromaWizard software (Auer et al., 2018) to
443 assign fluorescence colors to each chromosome. Based on these fluorescence
444 colors, the chromosome numbering was determined. Ten metaphase cells per
445 mouse were analyzed for karyotyping.
446
447 **Chromosome analysis by Giemsa banding (G-banding)**
448 When multicolor FISH analysis revealed a possible chromosome deletion,
449 additional G-band staining was performed to identify the lost part of the
450 chromosomes. The chromosome slides were treated with 0.025% trypsin
451 (FUJIFILM Wako Pure Chemical Corporation) for 2 min at room temperature,
452 washed in PBS, and stained with 4% Giemsa for 8 min. Deletion sites were
453 determined according to the band pattern nomenclature of mouse chromosomes
454 (Nesbitt and Francke, 1973).

455

456 **Live cell imaging**

457 After linearization of the template plasmids, mRNA was synthesized using the
458 mMESSAGE mMACHINE KIT (Ambion). The synthesized RNAs were stored at
459 −80 °C until use. The *in vitro*-transcribed mRNAs (1.2 pl of 650 ng/μl major
460 satellite-mClover (Miyanari et al., 2013) and 0.6 pl of 350 ng/μl H2B-mCherry)
461 were microinjected into oocytes. These were cultured for 1 hours and then
462 subjected to micromanipulation. Live cell imaging was performed as described
463 (Kitajima et al., 2011; Sakakibara et al., 2015), with some modifications. Briefly,
464 a Zeiss LSM710 or LSM880 confocal microscope equipped with a 40 ×
465 C-Apochromat 1.2NA water immersion objective lens (Carl Zeiss) was controlled
466 by a multi-position autofocus macro (Politi et al., 2018). For centromere tracking
467 (**Figure 3**), 19 confocal z-sections (every 1.5 μm) of 512 × 512 pixel x/y images
468 covering a total volume of 35.4 × 35.4 × 28.5 μm were acquired at 200-second
469 intervals for at least 10 hours after spermatocyte injection into oocytes
470 expressing major satellite-mClover and H2B-mCherry. Centromere tracking was
471 performed as described (Kitajima et al., 2011; Sakakibara et al., 2015). The
472 parental origin of chromosomes was identified by the intensities of the
473 chromosomes and the centromeres (lower fluorescent intensity for the
474 spermatocyte chromosomes) (**Figure S2A**).

475

476 **Statistical analysis**

The rates of chromosomal abnormalities and embryo development were evaluated using Fisher's exact probability test. The body and placental weights of pups were evaluated using Student's *t*-test.

SUPPLEMENTAL INFORMATION

Supplemental information can be found at ..

ACKNOWLEDGMENTS

This study was supported by KAKENHI Grant Numbers 23500507 (N.O.), JP19H05758 (A.O. and T.H.), 20H05376 (H.K.), and 18H05549 (T.S.K.).

AUTHOR CONTRIBUTIONS

N.O. and A.O. conceived the project. The project was developed jointly by A.O., T.K., S.M., H.T., T.S.K., and F.S. Experiments were carried out by N.O., T.H., H.K., Y.O., Y.F., and K.I. The paper was written by N.O., T.H., H.K., T.S.K., and A.O.

DECLARATION OF INTERESTS

The authors declare no competing interests.

495 **REFERENCES**

496 Akiyama, K., Akimaru, S., Asano, Y., Khalaj, M., Kiyosu, C., Masoudi, A.A.,
497 Takahashi, S., Katayama, K., Tsuji, T., Noguchi, J., and Kunieda, T. (2008). A
498 New ENU-Induced Mutant Mouse with Defective Spermatogenesis Caused by a
499 Nonsense Mutation of the Syntaxin 2/Epimorphin (*Stx2/Epim*) Gene. J.
500 Reprod.Dev. *58*, 122-128.

501 Auer, N., Hrdina, A., Hiremath, C., Vcelar, S., Baumann, M., Borth, N., and
502 Jadhav, V. (2018). ChromaWizard: An open source image analysis software for
503 multicolor fluorescence in situ hybridization analysis. Cytometry. Part A : the
504 journal of the International Society for Analytical Cytology *93*, 749-754.

505 Biswas, L., Tyc, K., El Yakoubi, W., Morgan, K., Xing, J., and Schindler, K.
506 (2021). Meiosis interrupted: the genetics of female infertility via meiotic failure.
507 Reproduction *161*, R13-r35.

508 Chatot, C.L., Lewis, J.L., Torres, I., and Ziomek, C.A. (1990). Development of
509 1-cell embryos from different strains of mice in CZB medium. Biol. Reprod. *42*,
510 432-440.

511 El Yakoubi, W., and Wassmann, K. (2017) Meiotic divisions: No place for gender
512 equality. Adv. Exp. Med. Biol. *1002*, 1-17.

513 Enguita-Marruedo, A., Sleddens-Linkels, E., Ooms, M., de Geus, V., Wilke, M.,
514 Blom, E., Dohle, G.R., Looijenga, L.H.J., van Cappellen, W., Baart, E.B., and
515 Baarends, W.M. (2019). Meiotic arrest occurs most frequently at metaphase and
516 is often incomplete in azoospermic men. Fertil. Steril. *112*, 1059-1070.

517 Fujiwara, Y., Ogonuki, N., Inoue, K., Ogura, A., Handel, M.A., Noguchi, J., and
518 Kunieda, T. (2013). t-SNARE Syntaxin2 (STX2) is implicated in intracellular
519 transport of sulfoglycolipids during meiotic prophase in mouse spermatogenesis.
520 Biol. Reprod. *88*, 141.

521 Fulka, H., and Langerova, A. (2014). The maternal nucleolus plays a key role in
522 centromere satellite maintenance during the oocyte to embryo transition.
523 Development *141*, 1694-1704.

524 Hayashi, K., Ohta, H., Kurimoto, K., Aramaki, S., and Saitou, M. (2011).
525 Reconstitution of the mouse germ cell specification pathway in culture by
526 pluripotent stem cells. Cell *146*, 519-532.

527 Hikabe, O., Hamazaki, N., Nagamatsu, G., Obata, Y., Hirao, Y., Hamada, N.,
528 Shimamoto, S., Imamura, T., Nakashima, K., Saitou, M., and Hayashi, K. (2016).
529 Reconstitution in vitro of the entire cycle of the mouse female germ line. Nature
530 *539*, 299-303.

531 Jamsai, D., and O'Bryan, M.K. (2011). Mouse models in male fertility research.
532 AsianJ. Androl. *13*, 139-151.

533 Kauppi, L., Barchi, M., Baudat, F., Romanienko, P.J., Keeney, S., and Jasin, M.
534 (2011). Distinct properties of the XY pseudoautosomal region crucial for male
535 meiosis. Science *331*, 916-920.

536 Kimura, Y., Tateno, H., Handel, M.A., and Yanagimachi, R. (1998). Factors
537 affecting meiotic and developmental competence of primary spermatocyte nuclei
538 injected into mouse oocytes. Biol. Reprod. *59*, 871-877.

539 Kitajima, T.S., Ohsugi, M., and Ellenberg, J. (2011). Complete kinetochore
540 tracking reveals error-prone homologous chromosome biorientation in
541 mammalian oocytes. Cell *146*, 568-581.

542 Kyogoku, H., and Kitajima, T.S. (2017). Large Cytoplasm Is Linked to the
543 Error-Prone Nature of Oocytes. Dev. Cell *41*, 287-298.

544 Lane, S.I.R., and Jones, K.T. (2017). Chromosome biorientation and APC
545 activity remain uncoupled in oocytes with reduced volume. J. Cell Biol. *216*,
546 3949-3957.

547 Ma, J.Y., Li, S., Chen, L.N., Schatten, H., Ou, X.H., and Sun, Q.Y. (2020). Why is
548 oocyte aneuploidy increased with maternal aging? J. Genet. Genomics *47*,
549 659-671.

550 Mihajlović A.I., and FitzHarris, G. (2018) Segregating chromosomes in the
551 mammalian oocyte. Curr. Biol. *28*, R895-R907.

552 Mikamo, K., and Kamiguchi, Y. (1983). A new assessment system for
553 chromosomal mutagenicity using chinese hamster oocytes and early zygotes. J.
554 Toxicol.Sci. *8*, 316.

555 Miki, H., Ogonuki, N., Inoue, K., Baba, T., and Ogura, A. (2006). Improvement of
556 cumulus-free oocyte maturation in vitro and its application to microinsemination
557 with primary spermatocytes in mice. J. Reprod. Dev. *52*, 239-248.

558 Mikwar, M., MacFarlane, A.J., Marchetti, F. Mechanisms of oocyte aneuploidy
559 associated with advanced maternal age. (2020) Mutat. Res. Rev. Mutat. Res.
560 *785*, 108320.

561 Miyanari, Y., Ziegler-Birling, C., and Torres-Padilla, M.E. (2013). Live
562 visualization of chromatin dynamics with fluorescent TALEs. Nat. Struct. Mol.
563 Biol. *20*, 1321-1324.

564 Nakamura, S., Kobori, Y., Ueda, Y., Tanaka, Y., Ishikawa, H., Yoshida, A.,
565 Katsumi, M., Saito, K., Nakamura, A., Ogata, T., et al. (2018). STX2 is a
566 causative gene for nonobstructive azoospermia. Hum. Mutat. *39*, 830-833.

567 Nesbitt, M.N., and Francke, U. (1973). A system of nomenclature for band
568 patterns of mouse chromosomes. Chromosoma *41*, 145-158.

569 Ogura, A., Matsuda, J., Asano, T., Suzuki, O., and Yanagimachi, R. (1996).
570 Mouse oocytes injected with cryopreserved round spermatids can develop into
571 normal offspring. J. Assist. Reprod. Genet. *13*, 431-434.

572 Ogura, A., Ogonuki, N., Miki, H., and Inoue, K. (2005). Microinsemination and
573 nuclear transfer using male germ cells. Int. Rev. Cytol. *246*, 189-229.

574 Ogura, A., Suzuki, O., Tanemura, K., Mochida, K., Kobayashi, Y., and Matsuda,
575 J. (1998). Development of normal mice from metaphase I oocytes fertilized with
576 primary spermatocytes. Proc. Nat. Acad. Sci. USA *95*, 5611-5615.

577 Ogura, A., and Yanagimachi, R. (1993). Round spermatid nuclei injected into
578 hamster oocytes form pronuclei and participate in syngamy. Biol.Reprod. *48*,
579 219-225.

580 Osawa, Y., Murata, K., Usui, M., Kuba, Y., Le, H.T., Mikami, N., Nakagawa, T.,
581 Daitoku, Y., Kato, K., Shawki, H.H., et al. (2021). EXOC1 plays an integral role in
582 spermatogonia pseudopod elongation and spermatocyte stable syncytium
583 formation in mice. eLife *10*.

584 Palermo, G., Joris, H., Devroey, P., and Van Steirteghem, A.C. (1992).
585 Pregnancies after intracytoplasmic injection of single spermatozoon into an
586 oocyte. Lancet *340*, 17-18.

587 Politi, A.Z., Cai, Y., Walther, N., Hossain, M.J., Koch, B., Wachsmuth, M., and
588 Ellenberg, J. (2018). Quantitative mapping of fluorescently tagged cellular
589 proteins using FCS-calibrated four-dimensional imaging. Nat. Protoc. *13*,
590 1445-1464.

591 Sakakibara, Y., Hashimoto, S., Nakaoka, Y., Kouznetsova, A., Höög, C., and
592 Kitajima, T.S. (2015). Bivalent separation into univalents precedes age-related
593 meiosis I errors in oocytes. Nat. Commun. *6*, 7550.

594 Skarnes, W.C., Rosen, B., West, A.P., Koutsourakis, M., Bushell, W., Iyer, V.,
595 Mujica, A.O., Thomas, M., Harrow, J., Cox, T., et al. (2011). A conditional
596 knockout resource for the genome-wide study of mouse gene function. Nature
597 *474*, 337-342.

598 Suzuki, H., Tsuda, M., Kiso, M., and Saga, Y. (2008). Nanos3 maintains the germ
599 cell lineage in the mouse by suppressing both Bax-dependent and -independent
600 apoptotic pathways. Dev. Biol. *318*, 133-142.

601 Tanaka, A., Suzuki, K., Nagayoshi, M., Tanaka, A., Takemoto, Y., Watanabe, S.,
602 Takeda, S., Irahara, M., Kuji, N., Yamagata, Z., and Yanagimachi, R. (2018).
603 Ninety babies born after round spermatid injection into oocytes: survey of their
604 development from fertilization to 2 years of age. Fertil. Steril. *110*, 443-451.

605 Tateno, H., and Kamiguchi, Y. (2007). Evaluation of chromosomal risk following
606 intracytoplasmic sperm injection in the mouse. Biol.Reprod. *77*, 336-342.
607
608

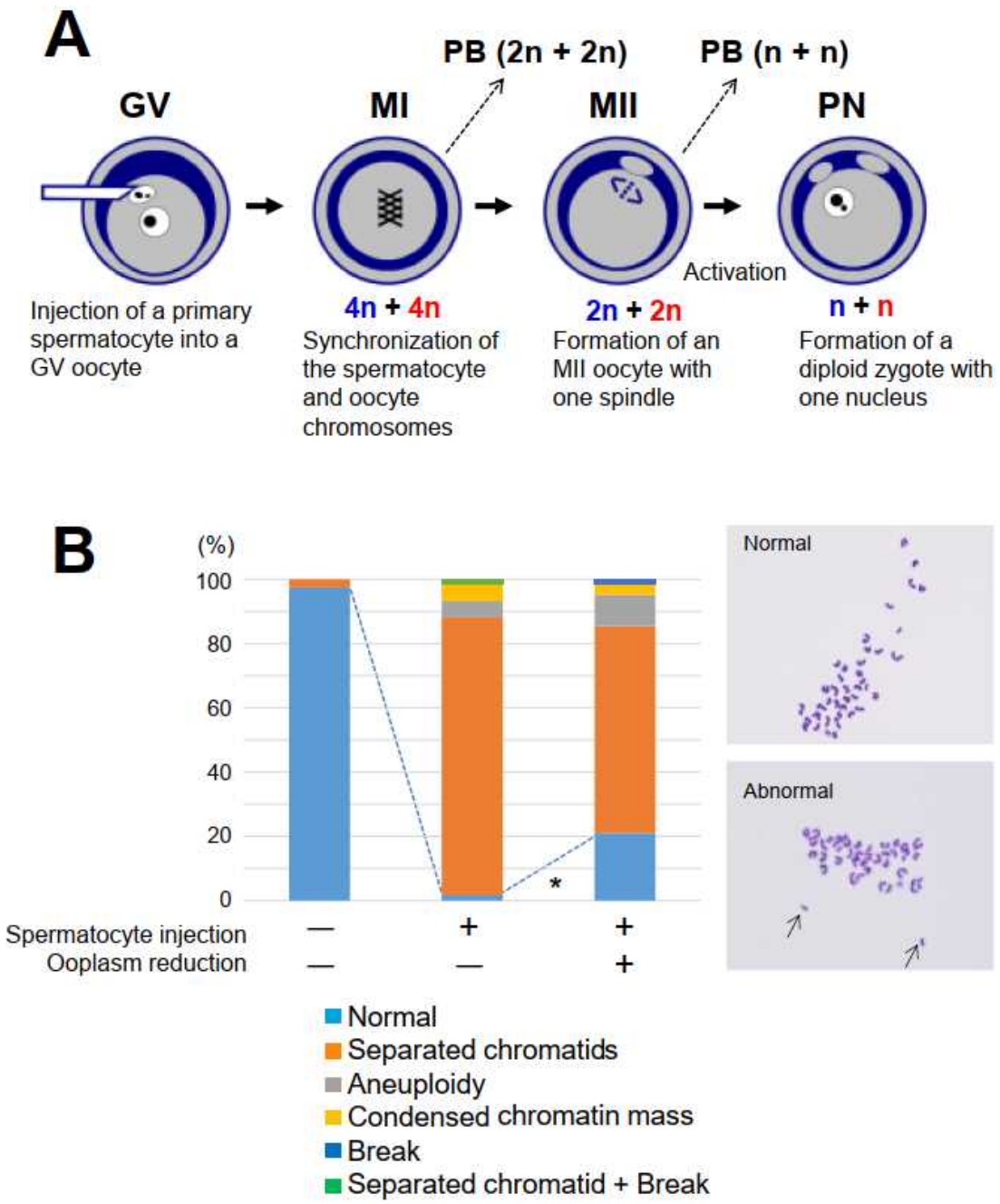
A
PB (2n + 2n)
PB (n + n)
GV
MI
MII
PN
Activation
Injection of a primary spermatocyte into a GV oocyte
4n + 4n
Synchronization of the spermatocyte and oocyte chromosomes
2n + 2n
Formation of an MII oocyte with one spindle
n + n
Formation of a diploid zygote with one nucleus
B
(%)
100
80
60
40
20
0
*
Spermatocyte injection
Ooplasm reduction
Normal
Abnormal
Normal
Separated chromatids
Aneuploidy
Condensed chromatin mass
Break
Separated chromatid + Break

609

610

611

612 **Figure 1. Fertilization with Primary Spermatocytes**

613 (A) The scheme of construction of a diploid fertilized oocyte using a primary
614 spermatocyte and a GV-stage oocyte. The chromosomes of the spermatocyte
615 and the oocyte are intermingled at MI to form a single chromosomal mass.
616 (B) Chromosomal analysis of MII oocytes that had been injected with primary
617 spermatocytes. In the spermatocyte-injected groups, normality was improved by
618 reducing the ooplasm mass (*$P < 0.005$ by Fisher's exact probability test).
619 Arrows in the right figure indicate prematurely separated chromatids. For the
620 exact numbers in each case, see also **Table S1**. PB, polar body; GV, germinal
621 vesicle; MI, meiosis I; PN, pronuclear stage.
622

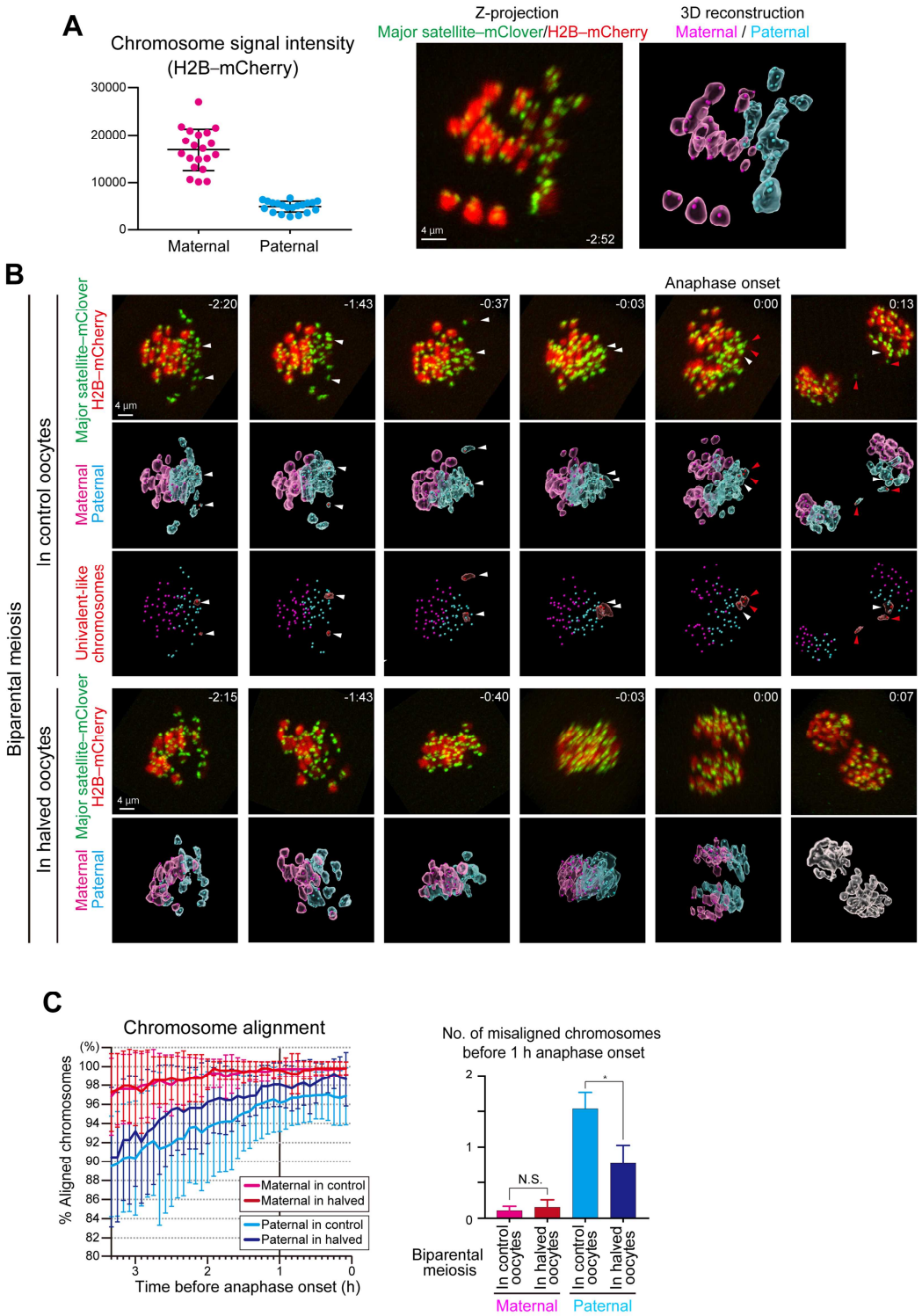
A
Chromosome signal intensity
(H2B–mCherry)
30000
20000
10000
0
Maternal
Paternal
Z-projection
Major satellite–mClover/H2B–mCherry
3D reconstruction
Maternal / Paternal
4 µm
-2:52
B
Anaphase onset
Biparental meiosis
In control oocytes
In halved oocytes
Major satellite–mClover
H2B–mCherry
Maternal
Paternal
Univalent-like
chromosomes
-2:20
-1:43
-0:37
-0:03
0:00
0:13
-2:15
-0:40
0:07
C
Chromosome alignment
(%)
% Aligned chromosomes
Time before anaphase onset (h)
Maternal in control
Maternal in halved
Paternal in control
Paternal in halved
No. of misaligned chromosomes
before 1 h anaphase onset
N.S.
*
Biparental
meiosis
In control
oocytes
In halved
oocytes
Maternal
Paternal

623

624

625 **Figure 2. Live Imaging of Biparental Meiosis**

626 (A) Identification of parental origin of the chromosomes was distinguishable
627 based on H2B-mCherry fluorescent intensities (paternal chromosomes exhibit
628 lower intensities). The z-projection image shows major satellite–mClover
629 (centromeres, green) and H2B-mCherry (chromosomes, red). Time from
630 anaphase onset is shown in h:min. Scale bar = 4 μm. The 3D-reconstructed
631 image shows maternal (magenta) and paternal (cyan) chromosomes. Spots
632 indicate centromeres.

633 (B) Chromosome tracking in 3D. The reconstructed images are viewed from the
634 side of the metaphase plate. Signals are interpolated in the Z axis for
635 visualization. White and red arrowheads, as well as red surfaces, indicate
636 univalent-like chromosomes that underwent unbalanced predivision (premature
637 segregation of sister chromatids). Scale bar = 4 μm.

638 (C) Halving the recipient ooplasmic mass rescued chromosome alignment. The
639 numbers of misaligned chromosomes and their parental origin were determined
640 in 3D (n = 39 and 17 oocytes). Error bars show the standard deviation. Student's
641 t test was used to compare means. *P < 0.05. N.S., not significant.

642

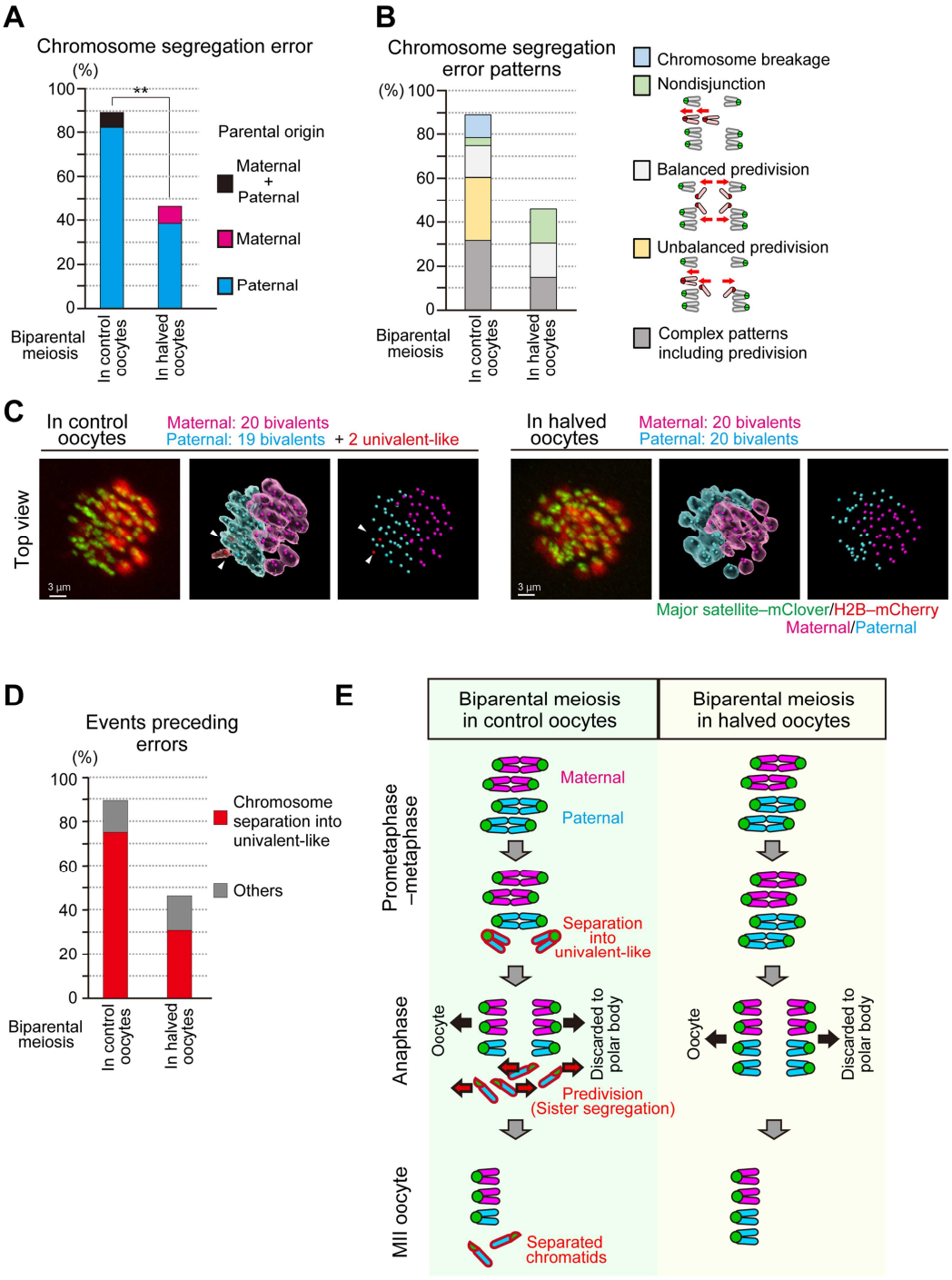
A
Chromosome segregation error
(%)
100
80
60
40
20
0
**
Parental origin
Maternal + Paternal
Maternal
Paternal
Biparental meiosis
In control oocytes
In halved oocytes
B
Chromosome segregation error patterns
(%) 100
80
60
40
20
0
Biparental meiosis
In control oocytes
In halved oocytes
Chromosome breakage
Nondisjunction
Balanced predivision
Unbalanced predivision
Complex patterns including predivision
C
In control oocytes
Maternal: 20 bivalents
Paternal: 19 bivalents + 2 univalent-like
In halved oocytes
Maternal: 20 bivalents
Paternal: 20 bivalents
Top view
3 µm
3 µm
Major satellite–mClover/H2B–mCherry
Maternal/Paternal
D
Events preceding errors
(%)
100
80
60
40
20
0
Chromosome separation into univalent-like
Others
Biparental meiosis
In control oocytes
In halved oocytes
E
Biparental meiosis in control oocytes
Biparental meiosis in halved oocytes
Prometaphase –metaphase
Maternal
Paternal
Separation into univalent-like
Anaphase
Oocyte
Discarded to polar body
Predivision (Sister segregation)
MII oocyte
Separated chromatids

643

644

645 **Figure 3. Halving the Recipient Ooplasm Prevents Premature Separation of**
646 **Paternal Chromosomes in Biparental Meiosis**
647 (A) Halving the recipient ooplasm mass reduced chromosome segregation
648 errors. Errors were determined by tracking all chromosomes at anaphase (n = 39
649 and 17 oocytes) (See also **Figure 2B**). The parental origin of errors is shown.
650 Ooplasmic halving significantly reduced the rate of errors (**P < 0.01).
651 (B) Predivision was predominant in biparental meiosis. Chromosome
652 segregation error patterns were categorized based on anaphase trajectories:
653 nondisjunction (0:4 segregation), balanced predivision (2:2 sister chromatid
654 segregation), unbalanced predivision (1:3 segregation including sister chromatid
655 segregation), and complex patterns including predivision (multiple errors
656 including sister chromatid segregation). Chromosome breakages (chromosomes
657 lacking centromeres) were also observed.
658 (C) Univalent-like chromosomes. Images were 3D-reconstructed as in Fig. 2B
659 and viewed from the top of the metaphase plate. Red surfaces with white
660 arrowheads indicate univalent-like chromosomes. Scale bar = 3 μm.
661 (D) Halving the ooplasm volume suppressed the premature separation of
662 paternal chromosomes. Oocytes were categorized based on whether the
663 chromosomes exhibited premature separation into univalent-like structures prior
664 to segregation errors.
665 (E) Summary of biparental meiosis. In normal-sized oocytes this frequently
666 exhibits premature separation of paternal chromosomes into univalent-like
667 structures. These chromosomes undergo predivision (premature segregation of
668 sister chromatids), and thus result in separated chromatids in MII oocytes.
669 Halving the ooplasmic volume reduced such errors.
670

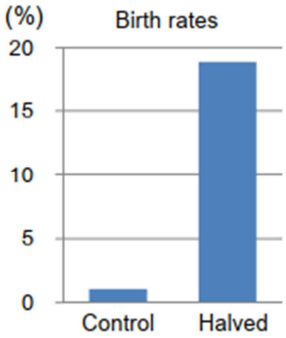

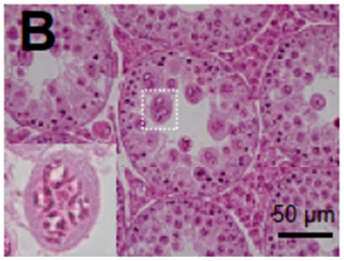

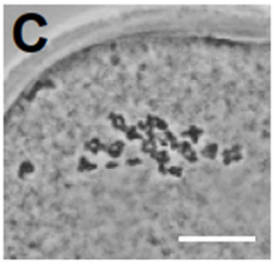

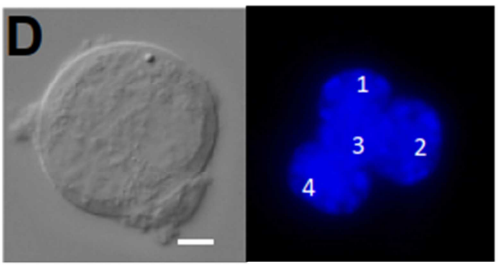

Birth of mice from *Stx2*^{repro34} mutant spermatocytes

No. oocytes cultured	No. (%) 2-cells	No. transferred	No. (%) implanted	No. (%) offspring	With mutation
133	75 (56)	41	19 (46)	5 (12)	5

Results from two replicated experiments

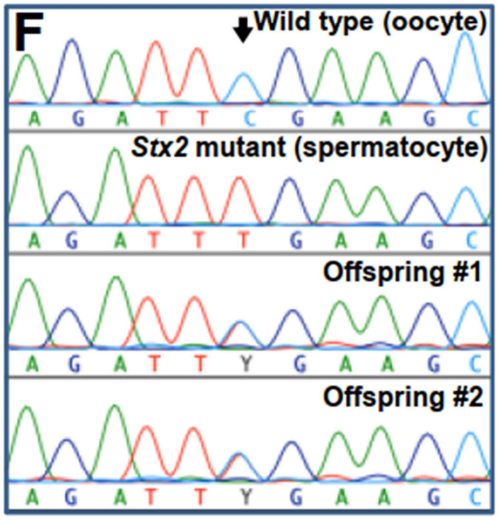

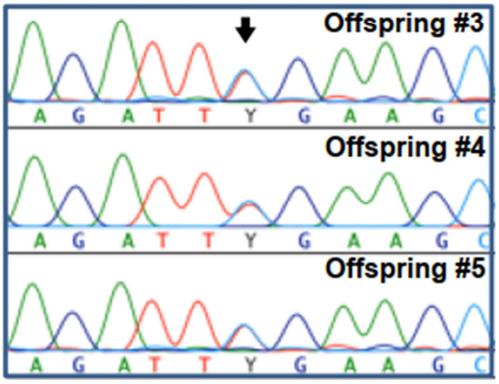

Fig. 4

671

672

673 **Figure 4. Birth of Spermatocyte-derived Offspring Following Embryo**
674 **Transfer**
675 (A) Mouse pups born following spermatocyte injection (left) and the birth rates
676 following embryo transfer (right). For detailed results, see also **Table S2**.
677 (B) Histology of the testis of a *Stx2*^{repro34} mouse. Arrowheads indicate
678 multinucleated cells containing spermatocyte-like nuclei. There are no
679 spermatids or spermatozoa. Bar = 50 μm.
680 (C) An MII oocyte injected with a putative spermatocyte nucleus from a
681 multinucleated cell in a *Stx2*^{repro34} mouse testis, showing the typical paired
682 meiotic chromosomes. Bar = 20 μm.
683 (D) A multinucleated cell isolated from a *Stx2*^{repro34} mouse testis, showing four
684 nuclei. Differential interference contrast (left) and Hoechst-stained (right)
685 images. Bar = 10 μm.
686 (E) (left) mouse pups born following microinjection with putative primary
687 spermatocyte nuclei isolated from multinucleated cells; (right) birth rate of pups
688 following *Stx2*^{repro34} spermatocyte microinjection.
689 (F) Genomic sequencing confirming the origin of pups from *Stx2*^{repro34}
690 spermatocytes. Arrows indicate the expected point mutation of *Stx2*^{repro34}. Y
691 indicates a hybrid status with T and C bases.
692